# Mitigating the effect of noise in the hybrid input–output method of phase retrieval

Russell Trahan III* and David Hyland

Department of Aerospace Engineering, Texas A&M University, HRBB 701, Ross Street, TAMU 3141, College Station, Texas 77843, USA

*Corresponding author: rtrahan3@tamu.edu

Received 11 February 2013; revised 27 March 2013; accepted 27 March 2013; posted 29 March 2013 (Doc. ID 185128); published 26 April 2013

Here a modification to the hybrid input–output (HIO) method of phase retrieval is presented which aides in mitigating the negative effects of low signal-to-noise ratios (SNRs). Various type of interferometers measure diffraction patterns which are used to determine the Fourier transform modulus of an objective. Interferometry often suffers from very low SNRs making phase retrieval difficult because of the sensitivity of most phase retrieval algorithms to local minima. Here we analyze the effect of noise on the HIO method. The result is used as a rationale for the proposed modification to the HIO method. The algorithm presented here introduces a filtering scheme which removes much of the Fourier modulus noise. Examples are shown and the results are compared to the HIO method with and without the proposed modification. Comparisons are also made to other methods of filtering the Fourier modulus noise. 

*OCIS codes:* (100.3020) Image reconstruction-restoration; (100.5070) Phase retrieval.
http://dx.doi.org/10.1364/AO.52.003031

## 1. Introduction

Many applications of phase retrieval suffer from low signal-to-noise ratio (SNR) levels in the acquisition of the Fourier modulus of the objective. A common method of phase retrieval in the fields of astronomy and microscopy is the hybrid input–output (HIO) algorithm as developed by Fienup [1]. This algorithm has been shown to recover an image from only its Fourier transform modulus. The performance of the HIO in the presence of noisy modulus data has been discussed; however, it does not have specific provisions for compensating for noise in the Fourier modulus data [2–5]. There have been very few proposed methods to filter noise from the modulus. A modification to the HIO was proposed by Liu [6,7], Bates and Mnyama [8], and Kohl *et al.* [9]. The algorithm in [9] is similar to the algorithm presented here, but has a difference in the implementation and rationale. The results by [6], [8], and [9] will be compared to the algorithm proposed here.

The HIO algorithm uses the image domain $f(x,y)$ and the image's Fourier domain $F(u,v)$ which are related by the Fourier transform

$$f(x,y) = F^{-1}\{|F(u,v)|\exp(i\varphi(u,v))\}, \tag{1}$$

where $F^{-1}\{\cdot\}$ is the two-dimensional inverse Fourier transform, $|F(u,v)|$ is the given modulus, and $\varphi(u,v)$ is the unknown phase. The HIO algorithm has four steps to determine the unknown phase starting with an initial guess of the image in $g_0(x,y)$. First, the image estimate $g_k(x,y)$ is Fourier transformed giving $G_k(u,v)$. Second, the input Fourier modulus $|F(u,v)|$ is imposed on $G_k(u,v)$ using

$$G'_k(u,v) = |F(u,v)|\exp(i\ \arg(G_k(u,v))). \tag{2}$$

Third, the result is inverse Fourier transformed, resulting in $g'_k(x,y)$. Lastly, the image is known *a priori* to be real valued, to be nonnegative, and possibly to

1559-128X/13/133031-07$15.00/0

have finite support. The next iteration's image is defined by

$$g_{k+1}(x,y) = \begin{cases} g'_k(x,y), & (x,y) \notin \gamma \\ g_k(x,y) - \beta g'_k(x,y), & (x,y) \in \gamma \end{cases}, \quad (3)$$

where $\gamma$ is the region of the image that is assumed to be background and $\beta$ is a feedback parameter.

As has been shown previously, the unique feature in the HIO is that the image's background constraint is not rigidly imposed, as is done in the Error-Reduction algorithm by Gerchberg and Saxton [10]. The HIO, rather, takes a gradient step toward imposing the background constraint. In a similar fashion, the HIO imposes the constraint that the image estimate has a Fourier transform modulus equal to a given input value. When this input Fourier modulus data contains noise, the HIO may not work properly.

The modulus noise may cause pixels in the background of the image to be nonzero even when the correct phase value has been estimated. Additionally, the modulus noise may cause pixels to be complex valued before the image domain constraint is applied even for proper phase estimates. The HIO, however, assumes that background pixels are, for the most part, zero and all pixels are real valued. As stated in [3] this can cause convergence issues, because the image and Fourier domain constraints contradict. The algorithm tends to oscillate between imposing the Fourier domain constraint and imposing the image domain constraint. The algorithm presented here will focus on filtering the noise, thus theoretically allowing all constraints to be satisfied simultaneously. In practice, this filtering would take infinite iterations, but the effects are significant within a very few iterations.

Figure 1, image (a) shows a sample image of a fictitious satellite. The image is $30 \times 30$ pixels with values ranging from 0 to 1. This image is used as a diagnostic because it has many background pixels not in $\gamma$, i.e., the foreground is concave. Also, the image is undersampled. Its autocorrelation exceeds the bounds of the $(u,v)$ plane. Figure 1, image (b) is after phase retrieval with the HIO with $\beta = 0.9$. The result is comparable to those typical of the HIO as shown in [2,8]. The Fourier modulus data was corrupted with random Gaussian noise according to

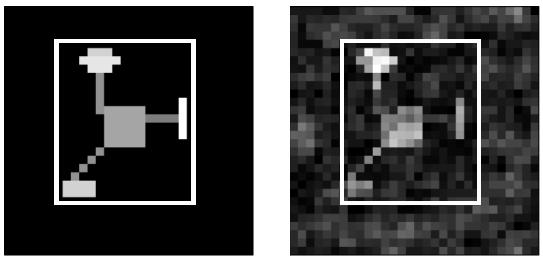

(a) True Image (b) Estimate, Iteration 500

Fig. 1. Example result used to demonstrate constraint oscillation in the HIO. The box indicates the boundary of $\gamma$.

$$\begin{aligned} |F(u,v)| &= |F(-u,-v)| \\ &= |F_{\text{True}}(u,v)(1 + N[0,\sigma] + N[0,\sigma]i)| \end{aligned} \quad (4)$$

with a standard deviation of $\sigma = 0.4$. Additionally, the symmetry of the $(u,v)$ plane was preserved. The model in Eq. (4) is a simplified model commonly used in intensity correlation interferometry for modeling the statistics of coherence magnitude measurements [11], which is based on the classical discussions in [12]. The Gaussian approximation is applicable because, in intensity correlation interferometry, several coherence magnitude estimates can be formed and averaged, thus invoking the central limit theorem which reduces the noise model to a Gaussian. The resulting corruption of the Fourier modulus data is comparable to many other models such as those in [1,2,7,8,13]. The noise level in this example represents a low enough SNR that convergence of the HIO is not guaranteed for every attempted initial condition; sometimes it stalls. The initial guess of the image used here is simply uniformly randomly distributed values.

A metric used to describe the modulus error is the sum of the deviation squared from the true modulus normalized by the dimension of the image $N$,

$$\tilde{E}_k^2 = N^{-2} \sum (|F_{\text{true}}(u,v)| - |G'_k(u,v)|)^2, \quad (5)$$

which in reality is unknown, but here it will provide a useful diagnostic. In this example, the modulus error is about 2.5. Shown in Fig. 2 is the norm of the image domain constraint violations,

$$e_k^2 = \sum_{\gamma} g_k(x,y)^2, \quad (6)$$

at each iteration. The constraint violations decrease by about half after the first 10 iterations as the image develops; however, convergence is quickly halted and an oscillation occurs. Figure 3 shows the norm of the Fourier modulus constraint violations,

$$E_k^2 = N^{-2} \sum (|G_k(u,v)| - F(u,v))^2, \quad (7)$$

at each iteration. It too stalls and oscillates as the image domain error does.

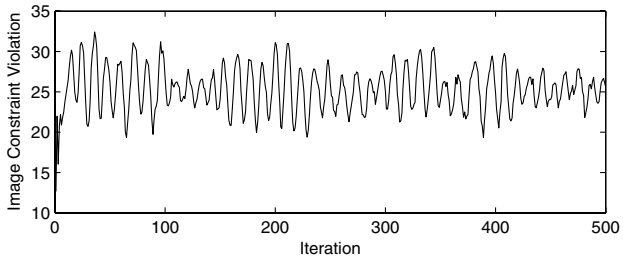


Fig. 2. Image constraint violation versus iteration for the HIO.

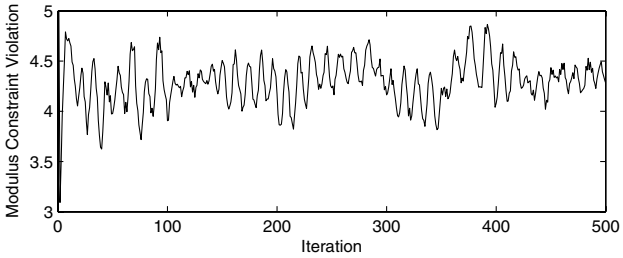


Fig. 3. Modulus constraint violation versus iteration for the HIO.

### A. Problem Statement

The oscillations in the image and Fourier domain constraint violations can be attributed to the idea that satisfying one constraint will cause a violation in the opposing constraint. A modification to the HIO is thus desired that can settle these oscillations and prevent the HIO from stalling at these high constraint violation levels by filtering the noise from the modulus data.

### B. Effect of Noise on the HIO

To gain insight into the effect of noise on the HIO, noise here is thought of as an addition of delta functions at various locations in the Fourier domain. The image and Fourier domains are considered discrete; therefore, the Fourier transforms between the two domains must be discrete.

If the true image's Fourier domain has values $F_{\text{True}}(u,v)$ for an image of dimensions $(M,N)$, then the noisy Fourier domain is

$$\tilde{G}(u,v) = F_{\text{True}}(u,v) + \sum_{(a,b)} \Delta(a,b)\delta(u-a,v-b). \quad (8)$$

In Eq. (8), $\Delta(a,b)$ is the magnitude of the noise component, and $a$ and $b$ are the UV plane locations of the noise component. Relating back to Eq. (4), $\Delta(u,v) = F(u,v) - F_{\text{True}}(u,v)$. This noise model can capture the statistics of any noise model as $\Delta(u,v)$ can be any value.

As a simplification, the linearity of the Fourier transform is exploited. Since the noisy Fourier domain is a sum of the image data and the noise, the noise is considered independent of the image's data. This assumption is valid for a Fourier transform, but not entirely valid for the HIO due to the image domain constraint being imposed on all of the image data and noise, not just the noise. Although not entirely valid for the HIO, this assumption gives valuable insight. Additionally, we are tracking only a single noise component to see the filtering effect, i.e., $(a,b)$, is constant here so let $\Delta(a,b) = \Delta$.

Considering the noise only, the Fourier domain before step 3 in the HIO is

$$G'(u,v) = \Delta\delta(u-a,v-b). \quad (9)$$

The inverse Fourier transform of this expression (step 3 in the HIO) is

$$f'(x,y) = \frac{\Delta}{MN} e^{2\pi i((ax/M)+(by/N))}, \quad (10)$$

for $x = [0, M-1]$ and $y = [0, N-1]$. In the HIO, the image is thought to be real valued, positive, and of finite support. If the image has nonzero pixels for $x = [A, M-1-A]$ and $y = [B, N-1-B]$, then the constrained image (step 4 in the HIO) is

$$f(x,y) = \begin{cases} |f'(x,y)|, & A \le m \le M-1-A \,\&\, B \le n \le N-1-B \\ 0, & \text{otherwise} \end{cases}$$
$$= \frac{\Delta}{MN} \begin{cases} 1, & A \le m \le M-1-A \,\&\, B \le n \le N-1-B \\ 0, & \text{otherwise} \end{cases}. \quad (11)$$

Note that $A$ and $B$ must be nonnegative. The corresponding discrete Fourier transform (after much algebraic simplification) is

$$G(u,v) = \frac{\Delta}{MN} \exp\left(i\pi\left(u\frac{M-4A-1}{M} + v\frac{N-4B-1}{N}\right)\right) \times \frac{\sin\left(\frac{M-2A}{M}\pi u\right)}{\sin\left(\frac{1}{M}\pi u\right)} \frac{\sin\left(\frac{N-2B}{N}\pi v\right)}{\sin\left(\frac{1}{N}\pi v\right)}. \quad (12)$$

The form of Eq. (12) resembles the *continuous* Fourier transform of rectangle functions which would be sinc functions in continuous space; however, the *discrete* Fourier transform adds the sin terms in the denominator making it the Dirichlet or "periodic sinc" function [14].

Since Eq. (12) is rather complex to analyze, consider its maximum magnitude,

$$G(0,0) = \Delta\frac{M-2A}{M}\frac{N-2B}{N}. \quad (13)$$

The maximum magnitude is proportional to the original noise magnitude $\Delta$ but is scaled by the factor

$$\frac{M-2A}{M}\frac{N-2B}{N}. \quad (14)$$

This attenuation factor shows that although more pixels in the Fourier domain are affected by the noise than in Eq. (9), the maximum magnitude is smaller.

For additional quantification of this attenuation that the HIO causes, consider the Frobenius norm of $|G(u,v)|$, which can be shown to be

$$\Delta\frac{M-2A}{M}\frac{N-2B}{N}, \quad (15)$$

opposed to the Frobenius norm of $|G'(u,v)|$, which is $\Delta$.

This result shows that the influence of the noise in the Fourier modulus is reduced proportional to the support of the image. Conceptually, if one thinks of

the power of the frequencies in $G'(u,v)$, the HIO essentially acts as a filter, thus reducing the total power contained within $G(u,v)$ due to the noise.

### 2. Constraint Relaxation

Previously, an iteration of the HIO equations was shown to reduce the power of noise in the Fourier modulus when going from $G'_k(u,v)$ to $G_{k+1}(u,v)$. With this effect in mind, it is proposed that $G_{k+1}(u,v)$ is a better estimate of the true Fourier modulus than $F(u,v)$. This thought implies that the Fourier modulus should be updated at every iteration to make $G'_k(u,v)$ resemble $G_k(u,v)$ more than $F(u,v)$. This update can be performed in a method similar to the image constraint in the HIO. Using the notation common in the HIO, the second step in the HIO should be

$$|G'_k(u,v)| = (1-\lambda)F(u,v) + \lambda|G_k(u,v)|. \tag{16}$$

Here $F(u,v)$ is the initial Fourier modulus on which we wish to perform phase retrieval, and $|G_k(u,v)|$ is the result of the HIO Fourier transform step at the current iteration. The name Constraint Relaxation is derived from the fact that the Fourier modulus at each iteration $|G'_k(u,v)|$ is not rigidly constrained to be the initial value $F(u,v)$. Rather, it is updated based on the current estimate with the relaxation parameter $\lambda$.

The choice for the value of $\lambda$ has two primary considerations. The first consideration is suppressing the oscillations in the image and Fourier domain constraint violations. The oscillations can be prevented for a value of $\lambda$ on the order of 0.01 to 0.001. For these small values of $\lambda$ the constraint is relaxed enough to create an intersection between the image and Fourier domain constraints. This relaxation is performed to aide in convergence, i.e., it can be performed starting at iteration one. The second consideration for choosing a $\lambda$ is filtering large amounts of Fourier modulus noise. To achieve noticeable filtering $\lambda$ should be between 0.5 and 1 (but not equal to unity). This large amount of relaxation should not be performed before the HIO has converged and stalled. Small values of $\lambda$ aide in convergence; large values of $\lambda$ can filter noise after convergence in addition to suppressing the constraint oscillations.

The form of (16) is similar to the method in [15]. The approach formulates the constraint relaxation with the intent of finding where the modulus and image domain constraints intersect. Here we maintain that with noise in the modulus, these two constraints may not intersect at all. Instead of seeking an intersection which may not exist, we wish to manipulate the data set to create an intersection by filtering the noise.

A method that is very close to the algorithm presented here is

$$|G'_k(u,v)| = (1-\lambda)|G_{k-1}(u,v)| + \lambda|G_k(u,v)|, \tag{17}$$

developed by Levi and Stark [16]. Similarly, Kohl's over-relaxation method of the form

$$G'_k(u,v) = (1-\lambda_A)G_k(u,v) + \lambda_A F(u,v)\exp(i\ \arg(G_k(u,v))) \tag{18}$$

is nearly identical to the one presented here except the relaxation parameter varies randomly at every iteration. They do not give a filtering style rationale because they do not consider modulus noise. They, like [15,17], were concerned with solving the HIO stagnation problem but not when the stagnation is caused by noise. In fact, they do not mention modulus noise in their algorithm's development. Additionally, the constraint given in Eq. (17) is vulnerable to instability. Since the initial value is not present in the constraint, the $|G'_k(u,v)|$ value can "run away." For the methods by Levi, Stark, and Kohl, comparisons will be given in a later section.

The algorithm presented here is uniquely developed with filtering noise in mind. Due to the similarities, the effect that it has on exiting local minima can be well explained by the comprehensive discussions in [9,15,16].

### 3. Examples

To show the effect constraint relaxation has on the HIO, the previous example in Fig. 1 was run for an additional 500 iterations. The constraint relaxation was implemented after iteration 500. The relaxation parameter $\lambda$ was set to 0.9.

Figure 4 shows (a) the image estimate just before the Fourier modulus constraint was relaxed and (b) after the relaxation was implemented for 500 iterations. The resulting image shows a few artifacts, but the image quality is indisputably better than the prerelaxation estimate, both in the foreground and background. Figure 5 shows the reduction in the image constraint violations. The oscillations cease, and the value decreases to nearly zero. The first iteration where the constraint relaxation is implemented sometimes yields a higher image constraint violation value, but the violations quickly decrease. Figure 6 shows the reduction in the Fourier modulus constraint violations.

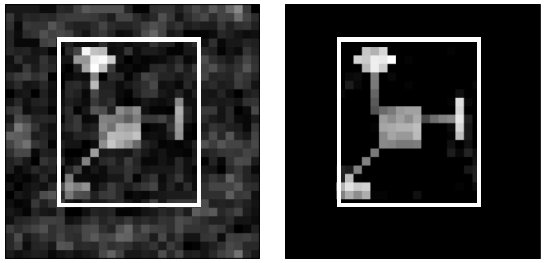

(a) Estimate, Iteration 500 (b) Estimate, Iteration 1000

Fig. 4. Image estimate comparison before and after the constraint relaxation was implemented. The box indicates the boundary of $\gamma$.

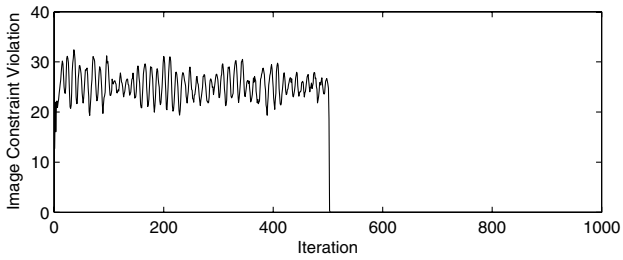


Fig. 5. Image constraint violation versus iteration. Constraint relaxation began at iteration 500.

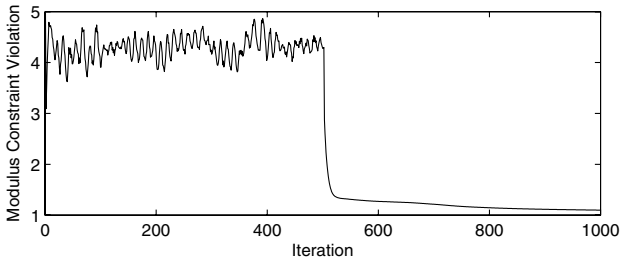


Fig. 6. Modulus constraint violation versus iteration. Constraint relaxation began at iteration 500.

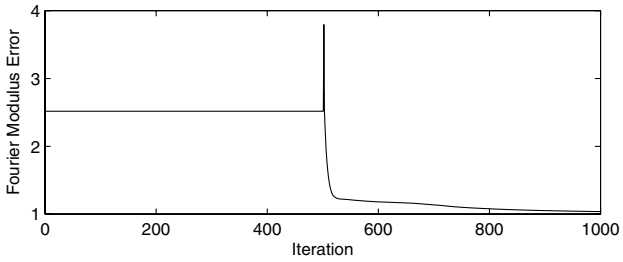


Fig. 7. Fourier modulus error versus iteration.

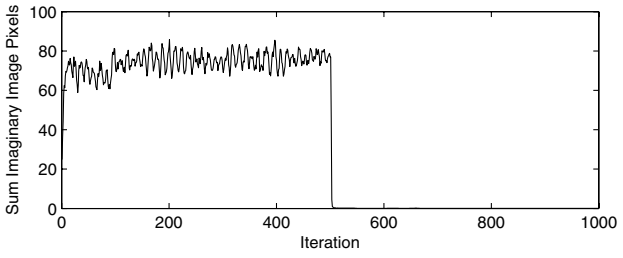


Fig. 8. Sum of the image's imaginary pixels prior to the image constraint being imposed versus iteration.

Figure 7 shows the Fourier modulus error defined by Eq. (5). Like the image constraint violations, a spike often occurs when the relaxation begins, but the value quickly decreases. The total noise reduction in this case is 62%. This is the most impressive result from the constraint relaxation, as this result shows that the value $|G'_k(u,v)|$ contains 62% less noise than the original input $|F(u,v)|$ when compared to $F_{\text{True}}(u,v)$. In various tests with the parameters and image used in this example, the noise reduction ranged from 30% up to 92%. This makes the example being shown here a nominal case.

An interesting effect that the relaxation has on the image is a reduction in the number of pixels that are complex valued prior to the image constraint being imposed. The quantity

$$\sqrt{\sum \arg\left(g'_k(u,v)\right)^2} \tag{19}$$

is reduced to nearly zero. In the example being discussed here, Fig. 8 shows this effect.

The previous example showed the image of a fictional satellite being reconstructed from its noisy Fourier modulus. To demonstrate the relaxed constraint method with a more realistic image, consider the image of Saturn in Fig. 9(a). The Fourier modulus is corrupted according to Eq. (4) in the same manner as the previous example with standard deviation of 0.4. The HIO was run without the constraint relaxation for 500 iterations, and the results are shown in Fig. 9(b).

The relaxation was again performed from iterations 500 to 1000 as shown in Fig. 9(c). The background region is nearly completely devoid of artifacts. The foreground is improved slightly, as shown by the planet's rings and silhouette being sharpened. The improvement of the foreground is not significant; however, the image is suffering from the convolution of the proper and flipped images. This is evident from the rings not being shown in front of the planet. Through methods such as those in [3,5,18–20] this can be corrected. Even with the flipped solution convolution, the Fourier modulus noise reduction was about 58%. With the addition of methods of obtaining a unique solution, which is beyond the scope of the discussions here, even more filtering is possible. We propose that algorithms such

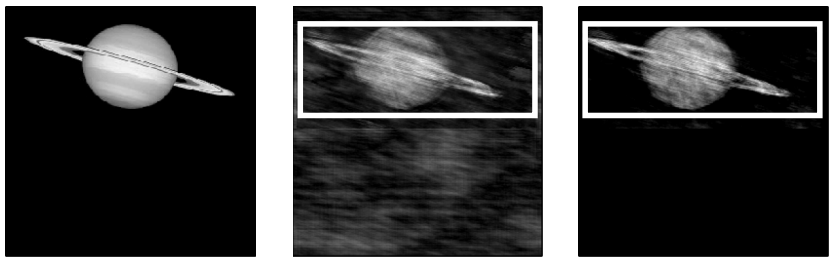


Fig. 9. Example result showing (a) the true image and (b) the reconstructed image after 500 iterations without constraint relaxation. The relaxation was performed from iteration 500 to 1000 with the result shown in (c). The box in (b) and (c) indicates the boundary of $\gamma$.

as those in [3,5,18–20], which better manage the flipping convolution and support issues, would provide far superior results if $|G'_{1000}(u,v)|$ were used as an input rather than $|F(u,v)|$, because the issue of conflicting image domain and Fourier domain constraint is nearly eliminated.

## 4. Conclusion

The objective here was to devise a modification to the HIO method of phase retrieval that not only tolerates noisy modulus data but is capable of filtering the noise. Filtering the noise was set as a goal to eliminate the oscillations in the image and Fourier domain errors and help prevent stagnation of the HIO. To develop a theoretical basis for a modification to the HIO, the effect that noise has on an iteration of the HIO was derived. This analysis showed that the HIO iteration provides an estimate of the modulus data that contains less noise than the measured modulus data. This result led to the development of the relaxed constraint algorithm. With the addition of the Fourier modulus constraint relaxation, the Frobenius norm of the error in the modulus data has been reduced by as much as 92% for noise levels high enough that the HIO alone was barely able to converge.

For comparison, the satellite example given here was run with various initial conditions and noise realizations using the method proposed in [6]. The resulting modulus error was reduced by at most 5% with an average reduction of 1%. The algorithm in [6] aides in convergence in the presence of noise but has not been shown as effective at filtering high amounts of noise in two-dimensional images. The algorithm proposed in [8] manages to filter some of the modulus noise by imposing a condition on the modulus based on the image's support. Namely, they rely on the image being largely oversampled. The algorithm presented here has no such requirement. In fact, the satellite image is undersampled, the autocorrelation extends beyond the measured $(u,v)$ domain. Large oversampling improves the performance here; however, it is not a requirement.

The phase retrieval algorithms presented in [9], [15], and [16] were discussed and shown to be similar to the algorithm presented here. These algorithms have extensive 'projection style' derivations and are shown to aide in eliminating local minimum induced stagnation. They, however, are not formulated to filter noise. The constraint relaxation by [16] is susceptible to instability when noise is present. In tests, we observed comparable noise reduction *if* the algorithm did not go unstable. At high noise levels, it was rare for the algorithm to not go unstable. For the satellite example given here, the noise reduction was only 32% using [16] as opposed to the 62%. Even when high levels of noise cancellation occurred, the filtering was still temporary. The error typically was decreased sharply when the relaxation was implemented, and afterward the error would steadily grow.

The relaxation method proposed in [9] performed very well with noiseless data but was never shown to exceed the noise cancellation seen by the algorithm presented here. Due to the randomization of the relaxation, the noise reduction drastically varied at each of the iterations. The noise reduction could possibly be as high as the reduction for the algorithm presented here but, unless the iterations were stopped when the random relaxation value was optimal, the noise reduction was small or the noise was made worse. These results exemplify our claim that the algorithm presented here is intended to filter noise where others do not have this intended purpose.

Other papers, such as [3,5,21], discuss noise levels with respect to phase retrieval. The algorithm proposed here differs from these in that not only is the algorithm able to converge in the present of a low SNR level, as many do, but the noise is actually filtered.

In the examples presented here, among others we have tried, the modulus constraint relaxation provides superior results when compared to other methods of phase retrieval with noisy data. With this form of constraint relaxation combined with more complex methods of determining the image's support and handling double images, phase retrieval surpassing the current state-of-the-field is possible. Future work on this topic includes prediction of the amount of noise reduction possible, extended testing with nonfinite support images, determination of optimal values for the relaxation parameter, and quantification of the oversampling benefits.

## References


1. J. R. Fienup, "Phase retrieval algorithms: a comparison," Appl. Opt. **21**, 2758–2769 (1982).
2. J. R. Fienup, "Reconstruction of an object from the modulus of its Fourier transform," Opt. Lett. **3**, 27–29 (1978).
3. J. R. Fienup and C. C. Wackerman, "Phase-retrieval stagnation problems and solutions," J. Opt. Soc. Am. A **3**, 1897–1907 (1986).
4. R. Bates, "Astronomical speckle imaging," Phys. Rep. **90**, 203–297 (1982).
5. S. Marchesini, H. He, H. N. Chapman, S. P. Hau-Riege, A. Noy, M. R. Howells, U. Weierstall, and J. Spence, "X-ray image reconstruction from a diffraction pattern alone," Phys. Rev. B **68**, 140101 (2003).
6. G. Liu, "Fourier phase retrieval algorithm with noise constraints," Signal Process. **21**, 339–347 (1990).
7. G. Liu, "Object reconstruction from noisy holograms: multiplicative noise model," Opt. Commun. **79**, 402–406 (1990).
8. R. Bates and D. Mnyama, "The status of practical Fourier phase retrieval," Adv. Electron. Electron Phys. **67**, 1–64 (1986).
9. M. Kohl, A. A. Minkevich, and T. Baumback, "Improved success rate and stability for phase retrieval by including randomized overrelaxation in the hybrid input output algorithm," Opt. Express **20**, 17093–17106 (2012).
10. R. W. Gerchberg and W. O. Saxton, "A practical algorithm for the determination of the phase from image and diffraction plane pictures," Optik **35**, 237–246 (1972).
11. D. Dravins, S. LeBohec, H. Jensen, and P. Nunez, "Optical intensity interferometry with the Cherenkov telescope array," Astropart. Phys. **43**, 331–347 (2012).

12. R. H. Brown and R. Q. Twiss, "The question of correlation between photons in coherent light rays," Nature **178**, 1447–1448 (1956).
13. C. M. Caves, "Quantum-mechanical noise in an interferometer," Phys. Rev. D **23**, 1693–1708 (1981).
14. A. V. Oppenhein and R. W. Schafer, *Discrete-Time Signal Processing*, 3rd ed. (Prentice-Hall, 1999).
15. S. Marchesini, "A unified evaluation of iterative projection algorithms for phase retrieval," Rev. Sci. Instrum. **78** 011301 (2007).
16. A. Levi and H. Stark, "Image restoration by the method of generalized projections with application to restoration from magnitude," J. Opt. Soc. Am. A **1**, 932–943 (1984).
17. V. Elser, "Phase retrieval by iterated projections," J. Opt. Soc. Am. A **20**, 40–55 (2003).
18. I. Kodama, M. Yamaguchi, N. Ohyama, T. Honda, K. Shinohara, A. Ito, T. Matsumura, K. Kinoshita, and K. Yada, "Image reconstruction from an in-line X-ray hologram," Opt. Commun. **125**, 36–42 (1996).
19. J. Zhao, D. Wang, F. Zhang, and Y. Wang, "Hybrid phase retrieval approach for reconstruction of in-line digital holograms without twin image," Opt. Eng. **50**, 091310 (2011).
20. J. S. Wu, U. Weierstall, and J. Spence, "Iterative phase retrieval without support," Opt. Lett. **29**, 2737–2739 (2004).
21. J. Miao, D. Sayre, and H. N. Chapman, "Phase retrieval from the magnitude of the Fourier," J. Opt. Soc. Am. A **15**, 1662–1669 (1998).